Research Article | Vol. 13, No. 8 / 1 Aug 2023 / Optical Materials Express 2227
Optical Materials EXPRESS

High-temperature electrical and optical properties of sputtered iridium at wavelengths of 300 nm to 15 µm

MINSU OH, JOHN MCELEARNEY, AND THOMAS E. VANDERVELDE*

Renewable Energy and Applied Photonics Labs, Department of Electrical and Computer Engineering, Tufts University, Medford, Massachusetts 02155, USA
tvanderv@ece.tufts.edu

Abstract: Due to its refractory properties and higher oxidation resistance, iridium (Ir) exhibits great potential for applications such as thermophotovoltaic emitters or contamination sensing. However, the lack of its temperature-dependent optical data prevents accurate modeling of Ir-based optical devices operating at higher temperatures. In this work, refractive indices of as-deposited and annealed Ir films, sputter-deposited, are characterized at between room temperature and 550°C over 300 nm to 15 µm of wavelength. The extinction coefficients of both as-deposited and annealed Ir films tend to decrease as temperature increases, with the exception of as-deposited Ir at 550°C due to significant grain growth. Under 530°C, optical constants of as-deposited Ir are less sensitive to temperature than those of annealed Ir. These characteristics of Ir films are correlated with their microstructural changes.

1. Introduction

Iridium (Ir) is known for its high melting point and oxidation resistance [1,2] – i.e. no oxide of Ir was detected after annealing in air at 400°C [1]. These properties make Ir an excellent candidate for applications such as thermophotovoltaic emitters [3–9] and contamination sensing [10]. However, the lack of temperature-dependent optical data of Ir [11–16] makes it challenging to model Ir-based optical devices for various temperatures with higher accuracy. Thus, knowledge of its temperature-dependent optical properties is essential to enable robust modeling. Thin layers of Ir can be deposited by varying techniques such as sputtering [14–16], atomic layer deposition (ALD) [15,17], or evaporation [13]. A recent work reports that high-density Ir film can be achieved at 10 mTorr ($\sim 1.3 \times 10^{-5}$ atm) argon (Ar) pressure [16]. In this work, optically thick Ir films were sputtered at 10 mTorr Ar pressure to obtain higher density. The optical and electrical properties of the films were characterized by spectroscopic ellipsometry at various temperatures over 300 nm to 15 µm of wavelength. The characteristics of their optical and electrical constants are correlated with microstructural changes such as void closure or grain growth.

The optical properties of conductors can be characterized by combining Lorentz, Gaussian [18], and Drude [19,20] oscillation models, which are temperature-dependent. The Lorentz and Gaussian models account for bound electrons, and the Drude model for free electrons. The response of free electrons to an electric field is determined by their scattering (or collision) characteristics at atomic lattice sites, surfaces, grain boundaries, impurities, and voids [21–24]. This indicates that optical properties of conductors are given as a function of temperature as well as microstructure. The relative permittivity (ε_r) of a conductor due to both bound and free electrons is expressed by

$$\varepsilon_r = \varepsilon_\infty + \sum \varepsilon_{bound} + \varepsilon_{Drude} \tag{1a}$$

$$\varepsilon_{Drude} = -\frac{1}{\varepsilon_0 \rho \tau}\left(\frac{1}{\omega^2 + i\frac{\omega}{\tau}}\right) \tag{1b}$$

#495250 https://doi.org/10.1364/OME.495250
Journal © 2023 Received 10 May 2023; revised 22 Jun 2023; accepted 25 Jun 2023; published 12 Jul 2023

Optical Materials EXPRESS

$$\rho = \frac{m^*}{Nq^2\tau}, \tag{1c}$$

where ε_∞: epsilon infinity (an offset by a purely real constant), ε_{bound} : permittivity contribution due to bound electrons, ε_{Drude}: permittivity contribution due to free electrons, ε_o: vacuum permittivity, ρ: direct-current (DC) resistivity, τ: mean scattering time, ω: angular frequency of light, m^*: effective electron mass, N: number of free electrons per unit volume, and q: magnitude of electron charge. Note that ρ and τ in Eq. (1) are effective terms accounting for all types of free electron scattering. For non-magnetic materials, their refractive index is obtained by the relationship $n + ik = \sqrt{\varepsilon_r}$, where n and k are real and imaginary parts of the refractive index, respectively. The imaginary part k is also referred to as extinction coefficient. The knowledge of refractive index allows calculation of several useful optical properties:

$$1 = R + T + A \tag{2a}$$

$$R = \frac{(n-1)^2 + k^2}{(n+1)^2 + k^2} \tag{2b}$$

$$A = \epsilon \tag{2c}$$

, where R: reflectance, T: transmittance, A: absorptivity (also called absorbance), and ϵ: emissivity. In Eq. (2a), the value of $R + T + A$ is equal to one due to the energy conversation law. We note that Eq. (2b) is for reflection at a planar interface between air and an optically thick material, where $T = 0$, at normal incidence [16]. In Eq. (2c), absorptivity and emissivity are equal to each other according to Kirchhoff's law [25,26]. If the transmittance is zero, then the emissivity is simply given by $\epsilon = 1 - R$.

2. Material preparation

A titanium (Ti) layer with a thickness of ~10 nm was deposited on a single crystalline silicon substrate, Si(100), as a buffer layer in a sputtering chamber (ATC Orion-3-HV, AJA International). After that, Ir was sputtered to the thickness of approximately 220 nm, measured by a profilometer (DektakXT, Bruker). The chamber pressure was 4.3×10^{-6} Torr (~5.7×10^{-9} atm) before the sputtering gas, Ar, was introduced into the chamber. Both Ti and Ir were deposited at room temperature. The sputtering parameters for Ir were: DC power 160 W and Ar pressure 10 mTorr (~1.3×10^{-5} atm). Both Ti and Ir targets were pre-sputtered for 2 min without a substrate in the chamber to clean the surfaces. After deposition of Ir, one half of the substrate was annealed at 700°C for 10 min in nitrogen (N_2) ambient –we note that an independent Ir sample annealed at 700°C for 12 hr under N_2 experienced surface quality degradation.

3. Results and discussion

3.1. Microstructure

The room-mean-square (RMS) surface roughnesses of Ir films were measured by atomic force microscopy (AFM) (Cypher, Asylum Research). The roughnesses were 1.4 nm for as-deposited and 2 nm for annealed samples; second order fit used over a 2 μm × 2 μm area. The Ir surfaces were also inspected by scanning electron microscopy (SEM) (Gemini 360, Zeiss) using secondary electron detection mode. The AFM and SEM images of as-deposited and annealed samples are shown in Fig. 1. It is evident that larger grains are formed in the annealed sample. The crystallinity of both films was inspected by grazing incidence x-ray diffraction (GIXRD) (SmartLab, Rigaku), shown in Fig. 2. The XRD peaks and corresponding crystal orientations of Ir and Ti thin films are well-identified in Refs. [27] and [28], respectively. The results of Fig. 1 and Fig. 2 suggest that the as-deposited and annealed Ir films are nanocrystalline and crystalline, respectively. The slight shifts of XRD peaks corresponding to Ir after annealing are attributed to stress release [29].

Optical Materials EXPRESS

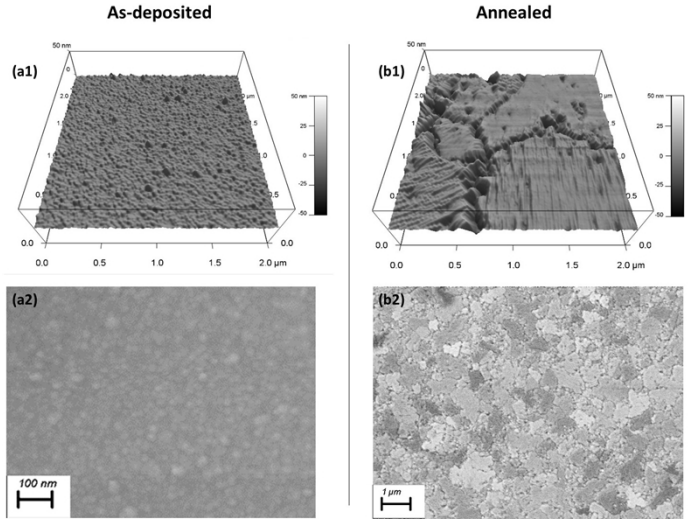

Fig. 1. AFM (top) and SEM (bottom) images of as-deposited and annealed Ir surfaces. Larger grains are formed in the annealed sample due to annealing effects. Both AFM and SEM images were taken at room temperature.

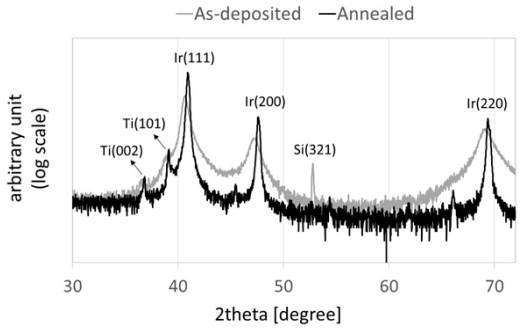

Fig. 2. GIXRD peaks of as-deposited and annealed Ir films at room temperature. The sharper peaks of the annealed sample suggest higher crystallinity due to larger grains. The shown Si(321) peak is due to the substrate, single crystalline silicon, which happened to be aligned for the peak. The XRD peaks and corresponding crystal orientations of Ir and Ti thin films are well-identified in Refs. [27] and [28], respectively.

Optical Materials EXPRESS

3.2. Optical properties

Prior to optical analysis, DC resistivities of as-deposited and annealed Ir films were measured by a four-point probe (Miller FPP-5000) at room temperature for Drude parameters. Optical data of the films, sample size 2 cm × 2 cm, were taken by spectroscopic ellipsometers (V-VASE and IR-VASE, J.A. Woollam) at the incidence angle 70° at various temperatures in N_2 ambient –the two ellipsometers measure different wavelength ranges. In both instruments, measurement was performed by increasing temperature from room temperature to 550°C. Independent samples were used for each ellipsometer to exclude annealing effects: one as-deposited Ir for V-VASE, another as-deposited Ir for IR-VASE, one annealed Ir for V-VASE, and another annealed Ir for IR-VASE. All scans started 6 min after the system reached the target temperature. We note that optical constants of Ir did not change significantly during measurements (details provided in Fig. S1 in Supplement Data). The data from both ellipsometers were modeled simultaneously without stitching them using the same oscillators –this technique is referred to as "multiple sample analysis" in the ellipsometer software WVASE. This was to independently fit incidence angles in the two instruments and acquire higher confidence in data fit. The Drude, Lorentz, and several Gaussian oscillators were used for modeling, where the epsilon infinity was fixed as one for all samples; $\varepsilon_\infty = 1$. We note that details about fit parameters and procedure are shown in Fig. S2 in Supplement Data. The resistivity measured by the four-point probe was used as a starting point for Drude parameters. When modeling, an additional layer was added on top of the Ir to incorporate the optical effects of surface roughness. This layer mixes Ir with voids at 50:50 volume percent, known as Bruggeman effective medium approximation. The surface roughness measured by AFM was used as the thickness of this layer. The fit parameters were independent of Ir thicknesses because our Ir films are optically thick and the reflection at the bottom of the Ir does not affect the measurement. Thus, the inclusion or exclusion of the Ti layer under Ir did not make a difference. The mean-squared error (MSE) between the data and fit was smaller than 1.33 for all measurements.

The refractive indices of Ir films measured at elevated temperatures are plotted in Fig. 3. The indices at room temperature agree with previously published values [14,15]. The temperature-dependent optical constants in this work are also provided in Tables S1 and S2 in Supplement Data. In Fig. 3, it is evident that extinction coefficients of as-deposited Ir are much smaller than those of annealed Ir at longer wavelengths. This is due to a larger content of voids/grain boundaries in the as-deposited film [13] –additional discussion on voids is provided in Fig. S3 in Supplement Data. At wavelengths below ~2 μm, however, there is no significant difference in the coefficient between the two samples. We speculate that this may be due to the geometry of void distribution –i.e. columnar structure of sputtered Ir [16]: Electrons may not have enough time to travel and collide with a void at shorter wavelengths. Moreover, the coefficients of both films tend to decrease as temperature increases. One exception to this is the as-deposited film at 550°C, as its coefficients at longer wavelengths are greater than those at 500°C. This is because of significant grain growth at 550°C, which will be discussed in Fig. 4. Additionally, under 500°C, as-deposited Ir exhibits lesser temperature-dependence of its refractive index than annealed Ir. This can be explained by accounting the opposite effects of temperature increase and void closure/grain growth on the Drude parameters in Eq. (1), which will be discussed in Fig. 6.

Figure 4(a) shows ellipsometric parameters of as-deposited Ir measured at between 500–550°C at a smaller temperature increment –the dwell time at each temperature was approximately 20 min. It is evident that the parameters at 550°C differ largely from those at other temperatures. SEM images of the Ir surface after measurements at 530°C and 550°C are shown in Fig. 4(b) and (c), respectively. The Ir after heating at 530°C is still nanocrystalline, similar to that of the as-deposited Ir in Fig. 1(a) that did not experience any heating. However, significant grain growth is observed after heating at 550°C. These results suggest that the sudden changes in optical properties of as-deposited Ir at 550°C is due to grain growth.

Optical Materials EXPRESS

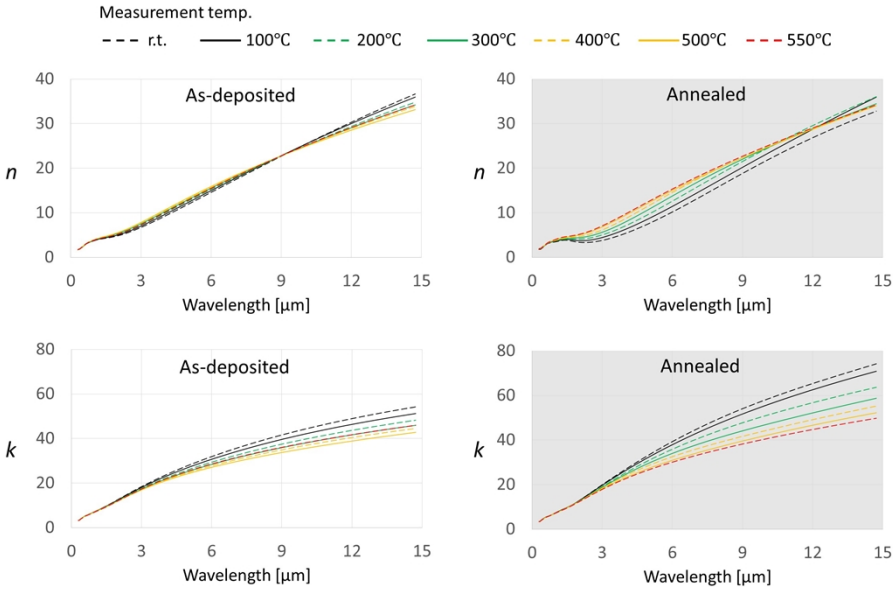

Fig. 3. Temperature-dependent refractive index of sputtered Ir. n and k are the real and imaginary parts, respectively. "r.t." in the legend stands for room temperature. A temperature variation leads to changes in refractive index as implied in Eq. (1).

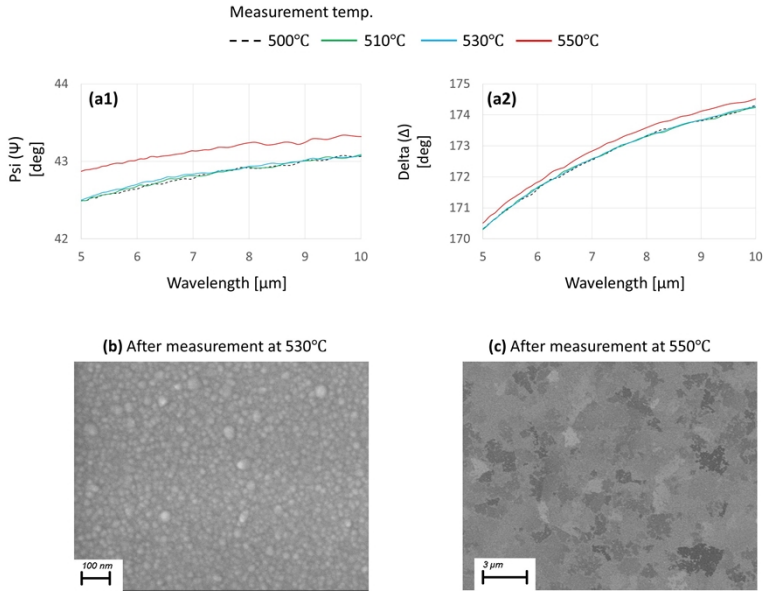

Fig. 4. As-deposited Ir. (a1) and (a2): ellipsometric parameters at temperatures between 500 - 550°C. (b): SEM image of the Ir sample for which the highest ellipsometric measurement temperature was 530°C. (c): SEM image of the Ir sample for which the highest ellipsometric measurement temperature was 550°C. All SEM images were taken at room temperature. Significant grain growth is observed in (c), which leads to sudden changes in optical properties.

Optical Materials EXPRESS

Furthermore, the measured refractive index was used to generate reflectance (R), absorptivity (A), and emissivity (ε) of optically thick Ir with zero surface roughness. Figure 5 shows the generated optical properties at normal incidence at various temperatures. The reflectance at room temperature agrees with previously published values [15]. It is evident that the reflectance of both as-deposited and annealed Ir at longer wavelengths decreases as temperature increases. One exception to this trend is the as-deposited film at 550°C, where the reflectance is higher than that at 500°C. These results are due to the temperature-dependent variation of refractive index, as can be inferred by Eq. (2b). Since the transmittance is zero for optically thick Ir, the absorptivity and emissivity in Fig. 5 were computed by the relationship $A = \varepsilon = 1 - R$, according to Eqs. (2a) and (2c). Both absorptivity and emissivity at longer wavelengths increase as temperature increases, with the exception of the as-deposited film at 550°C.

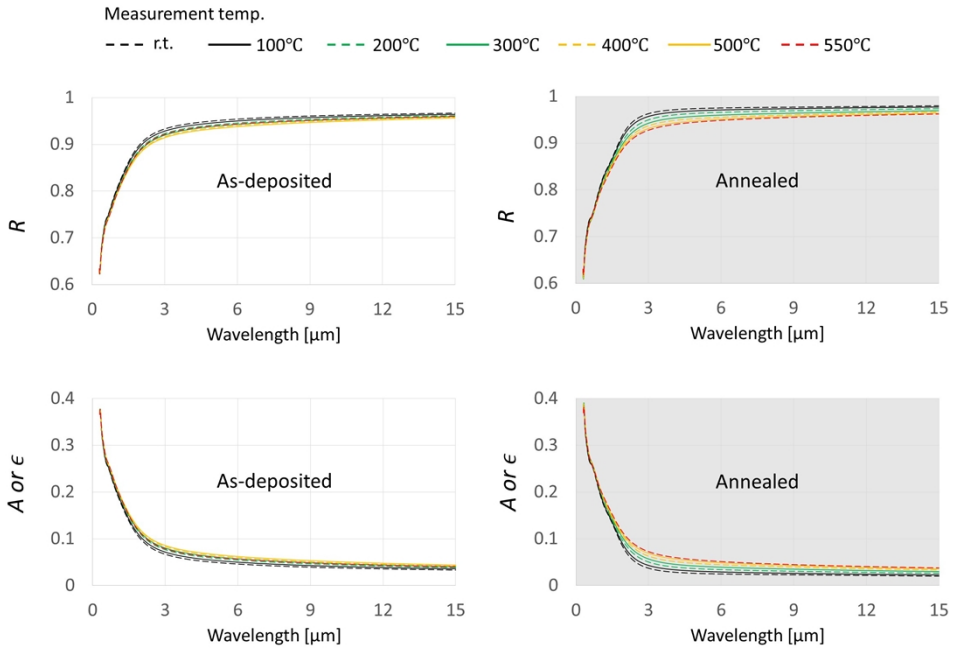

Fig. 5. Temperature-dependent optical properties of optically thick Ir with zero surface roughness at normal incidence. R: Reflectance, A: absorptivity, and ε: emissivity. "r.t." in the legend stands for room temperature. A temperature variation leads to changes in optical properties as implied in Eqs. (1) and (2).

3.3. Electrical properties

The resistivity and mean scattering time of Ir films were extracted from the measured Drude parameters at each temperature. These electrical properties are plotted in Fig. 6. In the figure, the resistivity of [Ir + Ti] layer measured by a four-point probe is also provided. We note that the four-point measurement of our Ir films was hardly affected by the thin Ti adhesion layer. At room temperature, the annealed film has a lower resistivity and a higher mean scattering time than those of the as-deposited. These results are attributed to void closure and larger grains due to annealing. For as-deposited Ir, at room temperature, optically (Drude) and directly (Four point) measured resistivities are quite different. This can be interpreted as that voids in the film affect the two measurement techniques differently. Both techniques, however, measured nearly the same resistivity of annealed Ir at room temperature. Moreover, the temperature-dependence of resistivity and scattering time of annealed Ir suggests that lattice scattering is dominant in the film

Optical Materials EXPRESS

[21]. In as-deposited Ir, an increase in temperature results in an increase in both resistivity and scattering time, up to 500°C. We interpret that the increase in scattering time is due to void closure as temperature starts to rise. Moreover, the fact that both resistivity and scattering time increase with temperature implies that the term $\frac{m^*}{N}$ for as-deposited Ir in Eq. (1c) increases as voids start to close. At 550°C, in the as-deposited film, however, both electrical properties have decreased. This can be interpreted as that the term $\frac{m^*}{N}$ decreases as a result of nanocrystalline-to-crystalline transition. Since the Drude model used in this work parameterizes only resistivity (ρ) and mean scattering time (τ) at a given wavelength, in Eq. (1b), the effective electron mass (m^*) and free electron density (N), in Eq. (1c), cannot be determined independently, which is not the focus of this work. The electrical properties in Fig. 6, however, are valid without knowledge of the value of m^* or N.

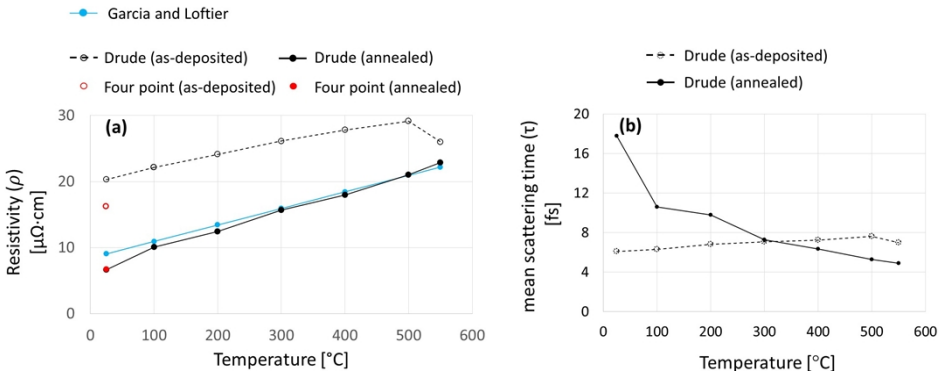

Fig. 6. Temperature-dependent DC resistivity (a) and mean scattering time (b) of Ir films. The parameters measured by spectroscopic ellipsometry and a four-point probe are denoted by "Drude" and "Four point", respectively. The Ir resistivity reported by Garcia and Loftier is from Ref. [30].

4. Conclusion

This work studied correlation between optical constants and microstructures of Ir as a function of temperature:

1) Significant grain growth occurs in the as-deposited Ir at between 530 - 550°C, which causes the extinction coefficients to increase.

2) Under 530°C, optical constants of as-deposited Ir are less sensitive to temperature variation than annealed Ir due to opposite effects of temperature increase and void closure on Drude parameters.

Thus, the results of this work provide fundamental data that are required to enable robust modeling of Ir-based optical devices for various temperatures.

Additionally, the resistivity of Ir films increases dramatically as the film thickness decreases below ~50 nm, due to surface scattering [31]. As resistivity affects optical properties, the extinction coefficients of extremely thin Ir films decrease as their thickness decreases [17]. This indicates that the optical constants of extremely thin Ir layers at higher temperatures are also influenced by their thickness. To correlate the refractive index of those Ir layers with their thickness and temperature, further study will be required.

Funding. National Science Foundation (ECCS-EPMD-2120568); Office of Naval Research (N00014-17-1-2591).

Optical Materials EXPRESS

Acknowledgments. The ellipsometry measurements were carried out at the Tufts Epitaxial Core Facility on equipment supported by the United States Office of Naval Research (No. ONR DURIP N00014-17-1-2591). This work was also completed in part at the Center for Nanoscale Systems (CNS) at Harvard University, a member of the National Nanotechnology Coordinated Infrastructure Network (NNCI), which is supported by the National Science Foundation under NSF Award No. 1541959. This work made use of the MRSEC Shared Experimental Facilities at MIT, supported by the National Science Foundation under award number DMR-1419807.

Disclosures. The authors declare no conflicts of interest.

Data availability. See Supplement 1 for supporting content.

Supplemental document. See Supplement 1 for supporting content.

References

1. S. Kohli, D. Niles, C. D. Rithner, and P. K. Dorhout, "Structural and optical properties of Iridium films annealed in air," Adv. X-ray Anal. **45**, 352–358 (2002).
2. M. Oh, J. McElearney, A. Lemire, and T. E. Vandervelde, "Material candidates for thermally robust applications of selective thermophotovoltaic emitters," Phys. Rev. Materials **6**(11), 110201 (2022).
3. M. Oh, E. S. Carlson, and T. E. Vandervelde, "Coupled resonance via localized surface plasmon polaritons in Iridium-based refractory metamaterials," Comput. Mater. Sci. **197**(May), 110598 (2021).
4. M. Oh, E. S. Carlson, and T. E. Vandervelde, "Localized surface plasmon resonance in refractory metamaterials," in *Advanced Fabrication Technologies for Micro/Nano Optics and Photonics XIV* (SPIE, 2021), 11696, p. 40.
5. T. Bauer, R. P. Forbes, and N. Pearsall, "The Potential of Thermophotovoltaic Heat Recovery for the Glass Industry," in *AIP Conference Proceedings* (AIP, 2003), 653, pp. 101–110.
6. L. M. Fraas, "Economic potential for thermophotovoltaic electric power generation in the steel industry," *2014 IEEE 40th Photovolt. Spec. Conf. PVSC 2014* 766–770 (2014).
7. T. Burger, C. Sempere, B. Roy-Layinde, and A. Lenert, "Present Efficiencies and Future Opportunities in Thermophotovoltaics," Joule **4**(8), 1660–1680 (2020).
8. W. E. S. W. A. Rashid, P. J. Ker, M. Z. Bin Jamaludin, M. M. A. Gamel, H. J. Lee, and N. B. A. Rahman, "Recent Development of Thermophotovoltaic System for Waste Heat Harvesting Application and Potential Implementation in Thermal Power Plant," IEEE Access **8**, 105156–105168 (2020).
9. M. M. A. Gamel, H. J. Lee, W. E. S. W. A. Rashid, P. J. Ker, L. K. Yau, M. A. Hannan, and M. Z. Jamaludin, "A Review on Thermophotovoltaic Cell and Its Applications in Energy Conversion: Issues and Recommendations," Materials **14**(17), 4944 (2021).
10. B. A. Banks, K. K. De Groh, E. Baney-Barton, E. A. Sechkar, P. K. Hunt, A. Willoughby, M. Bemer, S. Hope, J. Koo, C. Kaminski, and E. Youngstrom, *A Space Experiment to Measure the Atomic Oxygen Erosion of Polymers and Demonstrate a Technique to Identify Sources of Silicone Contamination* (NASA TM 1999–209180, 1999).
11. W. Haynes, D. Lide, and T. Bruno, *Handbook of Chemistry and Physics 97th Ed.* (CRC Press, 2016).
12. E. D. Palik, *Handbook of Optical Constants of Solids* (Academic Press, 1998).
13. G. Hass, G. F. Jacobus, and W. R. Hunter, "Optical Properties of Evaporated Iridium in the Vacuum Ultraviolet from 500 Å to 2000 Å," J. Opt. Soc. Am. **57**(6), 758 (1967).
14. L. Yan and J. A. Woollam, "Optical constants and roughness study of dc magnetron sputtered iridium films," J. Appl. Phys. (Melville, NY, U. S.) **92**(8), 4386–4392 (2002).
15. P. Schmitt, N. Felde, T. Döhring, M. Stollenwerk, I. Uschmann, K. Hanemann, M. Siegler, G. Klemm, N. Gratzke, A. Tünnermann, S. Schwinde, S. Schröder, and A. Szeghalmi, "Optical, structural, and functional properties of highly reflective and stable iridium mirror coatings for infrared applications," Opt. Mater. Express **12**(2), 545 (2022).
16. N. A. Pfiester, K. A. Grossklaus, M. A. Stevens, and T. E. Vandervelde, "Effect of microstructure on the optical properties of sputtered iridium thin films," Opt. Mater. Express **10**(4), 1120 (2020).
17. P. Schmitt, P. Paul, W. Li, Z. Wang, C. David, N. Daryakar, K. Hanemann, N. Felde, A. Munser, M. F. Kling, S. Schröder, A. Tünnermann, and A. Szeghalmi, "Linear and Nonlinear Optical Properties of Iridium Nanoparticles Grown via Atomic Layer Deposition," Coatings **13**(4), 787 (2023).
18. H. Fujiwara and R. W. Collins, *Spectroscopic Ellipsometry for Photovoltaics Volume 1: Fundamental Principles and Solar Cell Characterization* (Springer, 2018), 212.
19. H. Wang, K. Du, C. Jiang, Z. Yang, L. Ren, W. Zhang, S. J. Chua, and T. Mei, "Extended Drude Model for Intraband-Transition-Induced Optical Nonlinearity," Phys. Rev. Applied **11**(6), 064062 (2019).
20. H. Y. Li, S. M. Zhou, J. Li, Y. L. Chen, S. Y. Wang, Z. C. Shen, L. Y. Chen, H. Liu, and X. X. Zhang, "Analysis of the Drude model in metallic films," Appl. Opt. **40**(34), 6307 (2001).
21. S. O. Kasap, *Principles of Electronic Materials and Devices (Ch. 2)*, 3rd ed (McGraw-Hill Education, 2006).
22. J.-W. Lim and M. Isshiki, "Electrical resistivity of Cu films deposited by ion beam deposition: Effects of grain size, impurities, and morphological defect," J. Appl. Phys. **99**(9), 094909 (2006).
23. M. E. Day, M. Delfino, J. A. Fair, and W. Tsai, "Correlation of electrical resistivity and grain size in sputtered titanium films," Thin Solid Films **254**(1-2), 285–290 (1995).
24. T. Sun, B. Yao, A. P. Warren, K. Barmak, M. F. Toney, R. E. Peale, and K. R. Coffey, "Surface and grain-boundary scattering in nanometric Cu films," Phys. Rev. B **81**(15), 155454 (2010).

Optical Materials EXPRESS

25. T. Inoue, M. De Zoysa, T. Asano, and S. Noda, "Realization of narrowband thermal emission with optical nanostructures," Optica **2**(1), 27 (2015).
26. C. Shemelya, D. Demeo, N. P. Latham, X. Wu, C. Bingham, W. Padilla, and T. E. Vandervelde, "Stable high temperature metamaterial emitters for thermophotovoltaic applications," Appl. Phys. Lett. **104**(20), 201113 (2014).
27. X. Yan, T. Ai, X. Su, Z. Wang, G. Sun, and P. Zhao, "Synthesis and Thermal Decomposition Mechanism Study of a Novel Iridium Precursor," MATEC Web Conf. **43**, 01002 (2016).
28. N. J. Suliali, W. E. Goosen, A. Janse van Vuuren, E. J. Olivier, B. Bakhit, H. Högberg, V. Darakchieva, and J. R. Botha, "Ti thin films deposited by high-power impulse magnetron sputtering in an industrial system: Process parameters for a low surface roughness," Vacuum **195**, 110698 (2022).
29. M. Lee, *X-Ray Diffraction for Materials Research From Fundamentals to Applications (Ch. 6.4)*, 1st ed. (Apple Academic Press, 2016).
30. E. Yolanda García and D. G. Löffler, "Electrical Resistivities of Iridium, Palladium, Rhodium, and Tungsten at Temperatures between 295 and 1100 K," J. Chem. Eng. Data **30**(3), 304–305 (1985).
31. A. Jog and D. Gall, "Resistivity size effect in epitaxial iridium layers," J. Appl. Phys. **130**(11), 115103 (2021).